Extended Volume Image Reconstruction Using the Ellipse-Line-Ellipse Trajectory for a C-arm System

Zhicong Yu, Frédéric Noo, Günter Lauritsch, and Joachim Hornegger

***Abstract*—Recently, we proposed the Ellipse-Line-Ellipse trajectory for extended volume imaging with a C-arm system. Knowledge of the R-line coverage of this trajectory is well understood, but how to use the R-lines remains unclear. In this work, we establish a scheme for efficient and practical usage of the R-lines of this trajectory. Using computer-simulated data, we demonstrate this scheme by reconstruction results from the differentiated backprojection method.**

I. Introduction

We are interested in the development of extended volume cone beam (CB) computed tomography (CT) using the C-arm system in interventional radiology. For some intraoperative or emergency cases where the entire aorta or the spine needs to be examined, this tool could be crucial for patient health, particularly because it would prevent transferring the patient to the CT room, which is time consuming and increases risk to the patient.

Currently, C-arm systems employ a circular trajectory, which does not satisfy Tuy's condition and can not address extended volume imaging. A more sophisticated trajectory is needed. The helical trajectory has been successful in traditional CT systems, but it is not feasible on a C-arm system. Due to the open design and lack of slip-ring technology, a C-arm can not rotate infinitely in a single direction; in most cases, it can only allow a short scan. To overcome this mechanical limitation, the reverse helix [1] was proposed, which is like the helix, but reverses its rotational direction after a certain angular length. However, this trajectory does not have sufficient R-line coverage (An R-line is any segment of line that connects two source positions of the trajectory) in the middle of its convex hull, and thus theoretically-exact and stable (TES) reconstruction is challenging. Another possible solution would be the Arc-Line-Arc trajectory [2]. Nevertheless, this trajectory requires a full scan to achieve full R-line coverage in the region-of-interest (ROI), regardless of the size of the ROI, which is impractical for a C-arm system in most cases.

Recently, we have proposed a new geometry called the Ellipse-Line-Ellipse (ELE) trajectory [3], [4]. This trajectory possesses a reverse pattern in its rotational direction, and thus is feasible on a C-arm system. More importantly, we have proved that, through a simple configuration using a short scan, this trajectory provides sufficient R-lines for a typical cylindrical ROI that is centered on the patient table and inside the convex hull of the ELE trajectory.

At this stage, the R-line coverage of the ELE trajectory is well understood according to [3], [4], however, an efficient and practical scheme to select R-lines for TES image reconstruction yet needs to be established. In this work, we provide such a scheme for each point within the ROI such that the usage of the projection data varies smoothly when the point of interest in ROI moves continuously. We demonstrate this scheme by computer simulations using the method of differentiated backprojection followed by inverse Hilbert transform (DBP-HT) [5]. Reconstruction results show good image quality with smooth transition in transversal, coronal and sagittal directions.

Zhicong Yu and Frederic Noo are with Department of Radiology, University of Utah, Salt Lake City, UT, USA; Günter Lauritsch is with Siemens AG, Healthcare Sector, Forchheim, Germany; Zhicong Yu and Joachim Hornegger are with The Chair of Pattern Recognition, University of Erlangen-Nuremberg, Erlangen, Germany. This work was partially supported by a grant of Siemens AG, Healthcare Sector and by the U.S. National Institutes of Health (NIH) under grant R21 EB009168 and R01 EB007236. The concepts presented in this paper are based on research and are not commercially available. Its contents are solely the responsibility of the authors and do not necessarily represent the official views of the NIH.

II. The ELE trajectory

A. Geometry

The ELE trajectory lies on a cylindrical surface of radius R that is centered on the z-axis. This trajectory consists of two elliptical arcs connected by a segment of line as shown in the left of Figure 1, and we call the three components as the upper T-arc, T-line and the lower T-arc, respectively. In the attached (x, y, z)-coordinate system, the upper and lower T-arcs are mirror symmetric relative to the (x, y)-plane, and they lie in planes that are perpendicular to the (x, z)-plane, whereas the T-line is parallel to the z-axis; see the middle and right of Figure 1. Note that the ELE trajectory can be periodically repeated along the z-direction, and thus is suitable for extended volume imaging.

Let λ be the polar angle, and let γ_m be the fan-angle. We denote $\underline{a}_u(\lambda)$ and $\underline{a}_l(\lambda)$ as vertex points on the upper and lower T-arcs, respectively, and refer to $\underline{b}(z)$ as a vertex point on the T-line. By definition, we have

$$\begin{aligned}\underline{a}_u(\lambda) &= (R\cos\lambda, R\sin\lambda, H + \Delta H\cos\lambda),\\ \underline{b}(z) &= (R\cos\gamma_m, -R\sin\gamma_m, z),\\ \underline{a}_l(\lambda) &= (R\cos\lambda, R\sin\lambda, -H - \Delta H\cos\lambda),\end{aligned}$$

where $\lambda \in [-\gamma_m, \pi + \gamma_m]$ and $z \in [-H - \Delta H\cos\gamma_m, H + \Delta H\cos\gamma_m]$, with H and ΔH being configuration parameters as depicted in the right of Figure 1.

B. R-line coverage and ROI design

The R-line coverage of the ELE trajectory is composed of three parts, i.e., R-lines that are generated by connecting the

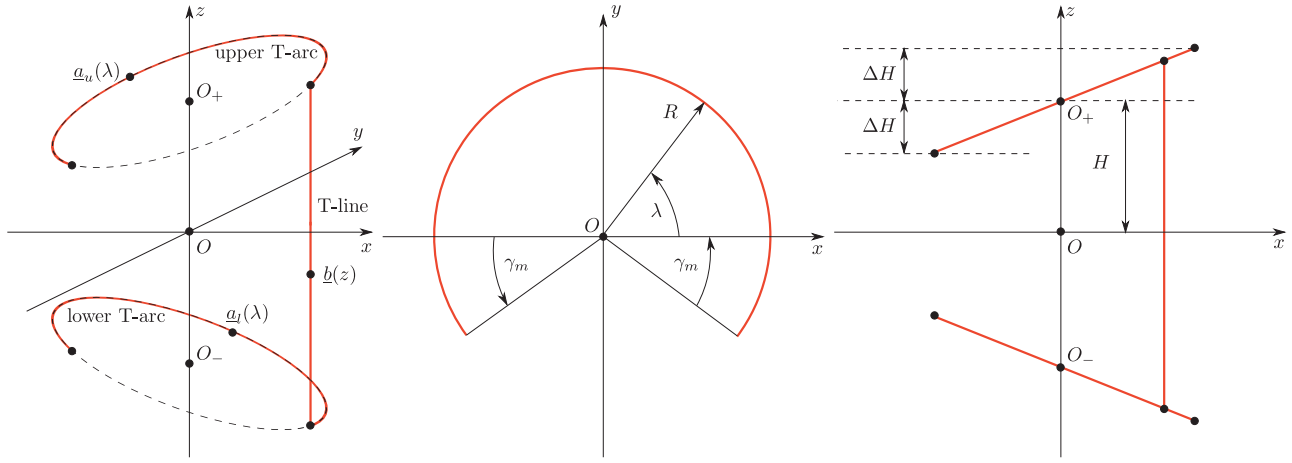

Fig. 1. Left: 3D illustration of the ELE trajectory. Middle: orthogonal projection onto the (x, y)-plane. Right: orthogonal projection onto the (x, z)-plane.

upper T-arc and the T-line (AL), the T-line and the lower T-arc (LA), as well as the upper and lower T-arcs (AA). Because the ELE trajectory is mirror symmetric relative to the (x, y)-plane, its R-line coverage is mirror symmetric as well. Hereafter, we will only focus on the R-line coverage for the space that is above the (x, y)-plane and within the convex hull of the ELE trajectory.

According to [4], for a given cylindrical ROI of radius $r < 0.85R$, full R-line coverage in the ROI can be guaranteed using the following configuration:

$$\gamma_m = \arcsin(r/R) \qquad \text{and} \qquad \Delta H/H = r/R.$$

C. Selection of R-lines

We define the surface generated by connecting one point on the T-line or the lower T-arc to all the points on the upper T-arc as the R-line surface, as shown in the left of Figure 2. When the convergent point of the R-line surface moves from the top point to the bottom point along the T-line, we obtain the blue R-line surfaces; whereas when the convergent point continues to move along the lower T-arc, we get the green R-line surfaces. We call the region covered by the R-line surfaces from the AL trajectory as the blue region, and refer to the region covered by the R-line surfaces from the AA trajectory as the green region.

It can be shown that when the convergent point on the lower T-arc reaches a certain polar position λ_c, every point in the ROI above the (x, y)-plane is covered by R-lines. For a typical ROI with radius $r < 0.5\,R$, $\lambda_c = 0$. Therefore, besides the upper T-arc and the T-line, only a small portion of the lower T-arc is needed for TES reconstruction in the ROI that is above the (x, y)-plane. In this work, for TES image reconstruction of the ROI above the (x, y)-plane, the R-lines forming the blue and green regions are selected.

The R-lines from the AL trajectory (blue) can cover a large portion of the ROI. However, in the first and second quadrants, some regions of the ROI are only covered by the R-lines from the AA trajectory, as shown in the middle of Figure 2. Let Q be a point in the green region, and refer to $\mathcal{L}(Q)$ as the line parallel to the z-axis that goes through Q, as shown in the right of Figure 2. As illustrated, the upper part (AB) of $\mathcal{L}(Q)$ is covered by the R-lines from the AL trajectory and the lower part (BC) is covered by the R-lines from the AA trajectory. Note that, C is not necessary the lowest point of the R-line coverage along $\mathcal{L}(Q)$ when the source position on the lower T-arc moves from $-\gamma_m$ to λ_c.

Some of the blue region is not only covered by R-lines from the AL trajectory, but also by the R-lines from the AA and LA trajectories. We disregard these contributions from the AA and LA trajectories so as to create a continuous scan and reconstruction flow. To the same reason, some of the green region is covered by two R-lines from the AA trajectory, but we only choose the one that has $\lambda \in [-\gamma_m, \lambda_c]$.

III. Reconstruction Method

Using the concept of an R-line surface, we perform the TES reconstruction using the DBP-HT method [5]. Let $\underline{x}$ be a 3D point, and $f(\underline{x})$ be the attenuation coefficient of the object at $\underline{x}$. We assume that $f(\underline{x})$ is compactly supported.

To perform the DBP-HT method in an efficient way, we now introduce a new coordinate system to describe the R-line surfaces, as shown in Figure 3. Let $\underline{b}(h)$ be a point on the T-line, and $\underline{a}_u(\lambda_*)$ be a point on the upper T-arc. We denote a point on the R-line that connects $\underline{b}(h)$ and $\underline{a}_u(\lambda_*)$ as $\underline{s}(h, \gamma, t)$. Let $\underline{\alpha}$ be the vector pointing from $\underline{b}(h)$ to $\underline{s}(h, \gamma, t)$, and refer to $\underline{\alpha}_{xy}$ as the orthogonal projection of $\underline{\alpha}$ onto the (x, y)-plane. Then γ and t are the polar angle and magnitude of $\underline{\alpha}_{xy}$, respectively. Because we are only interested in reconstructing the ROI, we have $\gamma \in [\pi - 2\gamma_m, \pi]$ and $t \in [R - r, R + r]$.

The coordinate system for describing the R-lines from the AA trajectory is similar to that from the AL trajectory, except that we use ω to indicate a point on the lower T-arc, i.e., $\underline{a}_l(\omega)$. For $r < 0.5R$, $\omega \in [-\gamma_m, 0]$. In this case, the range of γ is dependent on ω, i.e., $\gamma \in [\pi - \gamma_m + w, \pi + 0.5\gamma_m + 0.5\omega]$. The lower bound of γ is set to make sure that the ROI is covered by the R-line surfaces, whereas the upper bound of γ is set to make sure that the R-line surfaces do not include R-lines beyond the endpoint of the upper T-arc.

Based upon the above description, image reconstruction from the ELE trajectory using the DBP-HT method can be

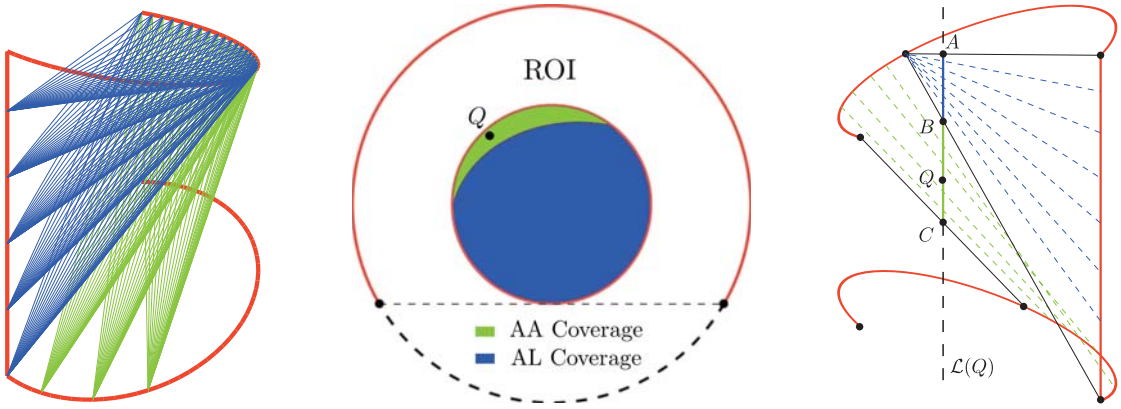

Fig. 2. Selection of the R-lines of the ELE trajectory for TES image reconstruction. Left: the R-line surfaces associated to the AL (blue) and AA (green) trajectories. Middle: the R-line coverage in the ROI in the (x, y)-plane. Right: R-line coverage along $\mathcal{L}(Q)$ that is from the AL (blue, composed of the upper T-arc and the T-line) and AA (green) trajectories.

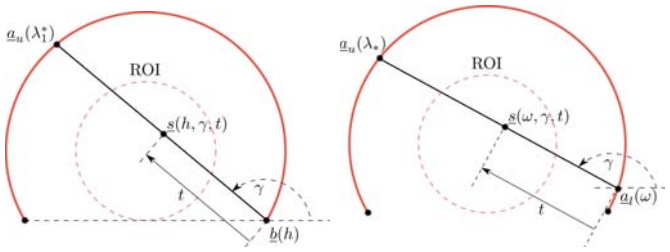

Fig. 3. The R-line surfaces of from the AL (left) and AA (right) trajectories can be described by (h, γ, t)- and (ω, γ, t)-coordinate systems, respectively.

achieved by the following steps.

- perform the view-dependent differentiation for all the projection data of the ELE trajectory;
- for each (h, γ, t) or (ω, γ, t), perform backprojection using the R-line segments that are selected in Section II-C;
- perform inverse Hilbert transform along t;
- rebin the reconstruction from the (h, γ, t)- or (ω, γ, t)-coordinate system to the (x, y, z)-coordinate system.

Among the four reconstruction steps, the rebin process deserves particular attention. For a given $\underline{x}$, if there is an R-line through this point from the AL trajectory, we should perform the rebinning from the (h, γ, t)-coordinate system to the (x, y, z)-coordinate system. Otherwise, we should perform the rebinning from the (ω, γ, t)-coordinate system to the (x, y, z)-coordinate system. The rebinning for the latter case is not trivial, and a detailed solution can be found in [4].

IV. Results

In this section, we present our numerical results using computer-simulated data. A modified FORBILD head phantom was adopted for data simulation. This phantom was obtained by stretching most of the FORBILD head phantom in the x-direction by a factor of 1.25, so that the horizontal slices of this phantom is circular, as shown in Figure 4. This modification was made for a better illustration of the reconstruction results from the AA trajectory.

The largest slice of the modified phantom appears at $z = 0$ cm with radius 12 cm, which, therefore, was set as the radius

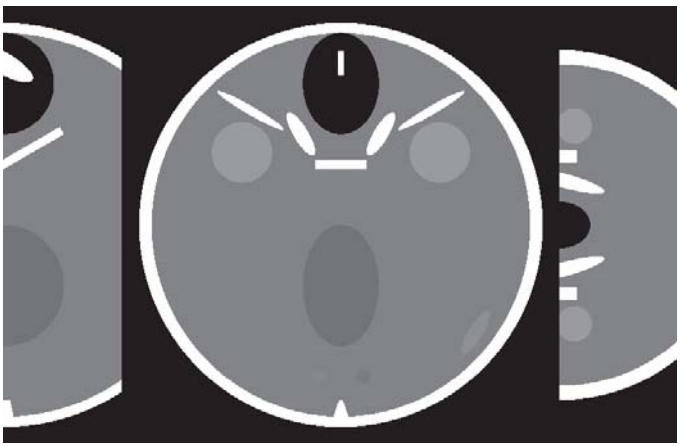

Fig. 4. The modified FORBILD head phantom. Left: sagittal slice at $x = 0$ cm with $z \in [0, 7]$ cm. Middle: transversal view at $z = 0$ cm. Right: coronal view at $y = 6$ cm with $z \in [0, 7]$ cm. Display window: $[0, 100]$ HU.

of the ROI. For data acquisition, a flat panel detector of bin size $0.06\,\text{cm} \times 0.06\,\text{cm}$ was used. This detector was large enough to avoid truncation. The scan radius was 30 cm, and the source-to-detector distance was 45 cm.

Regarding the ELE trajectory, we chose $H = 5$ cm and $\Delta H = 2$ cm so that R-line coverage was sufficient in the ROI. For each of the upper and lower T-arcs, 500 CB projections were generated over the angular range $[-24°, 204°]$, whereas for the T-line, 51 CB projections were generated. Note that the z-range of the T-line was automatically generated using H, ΔH and the angular range of the T-arcs. All CB projections were acquired using quarter detector pixel shift.

Regarding the DBP-HT reconstruction algorithm, we implemented the view-dependent differentiation according the the scheme presented in [6]. The resolution control parameter ε used in our experiment was 0.001. The inverse Hilbert transform was implemented according to Equation 18 of [7], and the constant C_t in this equation was calculated using Equation 20 from the same paper.

Reconstructions on the R-line surfaces from the AL and AA trajectories are shown in Figure 5. For the AL trajectory,

we selected 200 R-line surfaces with their convergent points evenly distributed along the T-line. For each AL R-line surface, 900 points were sampled evenly for γ over the range $[132°, 180°]$, whereas 900 points were sampled for t over the range $[16.5\,\text{cm}, 33.5\,\text{cm}]$. For the AA trajectory, we selected 225 R-line surfaces with their convergent points uniformly distributed along the lower T-arc over the range $[-24°, 0°]$. For each w, we evenly sampled 900 points for γ over the range $[\pi - \gamma_m + w, \pi + \gamma_m + w]$, with $\gamma_m = 24\pi/180$. The grid for t was the same as that of the R-line surfaces from the AL trajectory.

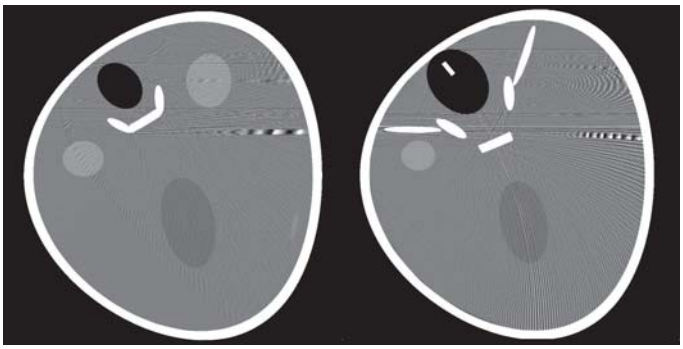

Fig. 5. Left: the reconstruction on the R-line surface at $h = 0.0343\,\text{cm}$. Right: the reconstruction on the R-line surface at $w = -22.4°$. Display window: $[0, 100]$ HU.

We obtained the final image reconstruction through rebinning using triple linear interpolation with isotropical voxels of size $0.02\,\text{cm}\times0.02\,\text{cm}\times0.02\,\text{cm}$. Part of the final image was rebinned from the AL trajectory, and the rest was rebinned from the AA trajectory. The rebinned images at $z = 0\,\text{cm}$ from the AL and AA trajectories are shown in Figure 6. The final rebinned results by using both AA and AL trajectories are shown in Figure 7. As illustrated, the final reconstruction results have good image quality with smooth transition in coronal, sagittal and transversal directions.

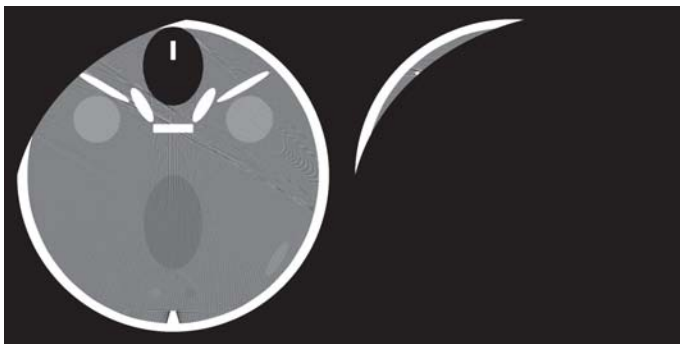

Fig. 6. Left: image rebinned from the R-line surfaces of the AL trajectory. Right: image rebinned from the R-line surfaces of the AA trajectory. Image position: $z = 0\,\text{cm}$. Display window: $[0, 100]$ HU.

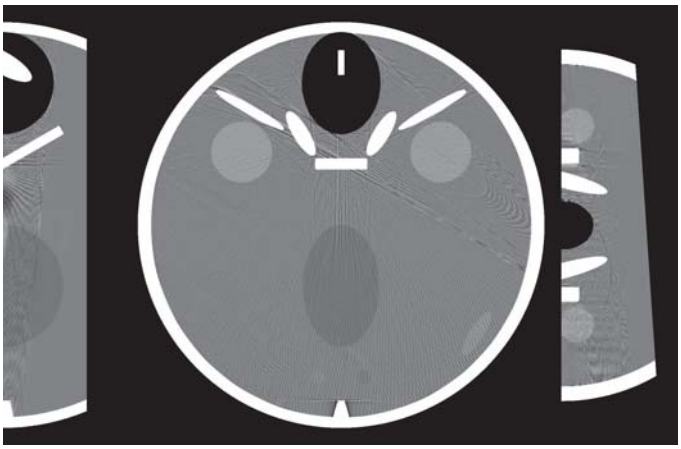

Fig. 7. Final image reconstruction rebinned through triple linear interpolation using isotropical voxels of size $0.02\,\text{cm}\times0.02\,\text{cm}\times0.02\,\text{cm}$. Top: sagittal view at $x = 0\,\text{cm}$. Middle: transversal view at $z = 0$. Bottom: coronal view at $y = 6\,\text{cm}$. Display window: $[0, 100]$ HU.

V. Conclusion and discussion

We have proposed an efficient and practical method to use the R-lines of the ELE trajectory for TES image reconstruction. For reconstruction of the ROI above the (x, y)-plane, besides the upper T-arc and the T-line, only a small continuous portion of the lower T-arc that is connected to the T-line is needed.

Although we only demonstrated how to address the R-lines for the ROI above the (x, y)-plane, it is straight forward to extend this method to the whole ELE trajectory as well as its duplicates. Also note that, in this work, we have used the DBP-HT method for image reconstruction, however, other TES methods such as Katsevich-type algorithms are also applicable.

References

[1] S. Cho, D. Xia, C. A. Pellizzari, and X. Pan, "A BPF-FBP tandem algorithm for image reconstruction in reverse helical cone-beam CT," *Med. Phys.*, vol. 37, no. 1, pp. 32–39, Jan 2010.

[2] Z. Yu, A. Wunderlich, F. Dennerlein, G. Lauritsch, and F. Noo, "Line plus arc source trajectories and their r-line coverage for long-object cone-beam imaging with a c-arm system," *Phys. Med. Biol.*, vol. 56, no. 12, p. 3447, 2011.

[3] Z. Yu, F. Noo, G. Lauritsch, F. Dennerlein, and J. Hornegger, "Ellipse-line-ellipse source trajectory and its r-line coverage for long-object cone-beam imaging with a c-arm system," in *SPIE Conference Series*, vol. 8313, 2012, p. 117.

[4] Z. Yu, F. Noo, Y. Mao, F. Dennerlein, G. Lauritsch, and J. Hornegger, "Ellipse-line-ellipse source trajectory and its r-line coverage for extended volume imaging using a c-arm system," *In preparation for submission to Phys. Med. Biol.*

[5] H. Schöndube, *Helical Cone-Beam Computed Tomography using the Differentiated Backprojection*. Shaker Verlag, Aachen, Germany, 2010.

[6] F. Noo, S. Hoppe, F. Dennerlein, G. Lauritsch, and J. Hornegger, "A new scheme for view-dependent data differentiation in fan-beam and cone-beam computed tomography," *Phys. Med. Biol.*, vol. 52, no. 17, p. 5393, 2007.

[7] F. Noo, R. Clackdoyle, and J. Pack, "A two-step hilbert transform method for 2d image reconstruction," *Phys. Med. Biol.*, vol. 49, no. 17, p. 3903, 2004.